Electronic Origin of Optically-Induced Sub-Picosecond Lattice Dynamics in MoSe₂ Monolayer

Lindsay Bassman,[†,‡] Aravind Krishnamoorthy,[†] Hiroyuki Kumazoe,[#] Masaaki Misawa,[#] Fuyuki Shimojo,[#] Rajiv K. Kalia,[†,‡,§,∥] Aiichiro Nakano,[†,‡,§,∥,⊥] and Priya Vashishta*,[†,‡,§,∥]

[†]Collaboratory for Advanced Computing and Simulations, [‡]Department of Physics and Astronomy, [§]Department of Computer Science, [∥]Department of Chemical Engineering and Material Science, and [⊥]Department of Biological Sciences, University of Southern California, Los Angeles, California 90089-0242, United States
[#]Department of Physics, Kumamoto University, Kumamoto 860-8555, Japan

S *Supporting Information*

ABSTRACT: Atomically thin layers of transition metal dichalcogenide (TMDC) semiconductors exhibit outstanding electronic and optical properties, with numerous applications such as valleytronics. While unusually rapid and efficient transfer of photoexcitation energy to atomic vibrations was found in recent experiments, its electronic origin remains unknown. Here, we study the lattice dynamics induced by electronic excitation in a model TMDC monolayer, MoSe₂, using nonadiabatic quantum molecular dynamics simulations. Simulation results show sub-picosecond disordering of the lattice upon photoexcitation, as measured by the Debye−Waller factor, as well as increasing disorder for higher densities

of photogenerated electron−hole pairs. Detailed analysis shows that the rapid, photoinduced lattice dynamics are due to phonon-mode softening, which in turn arises from electronic Fermi surface nesting. Such mechanistic understanding can help guide optical control of material properties for functionalizing TMDC layers, enabling emerging applications such as phase change memories and neuromorphic computing.

KEYWORDS: MoSe₂, structural dynamics, TMDC, 2D materials, nonadiabatic quantum molecular dynamics, electronic structure
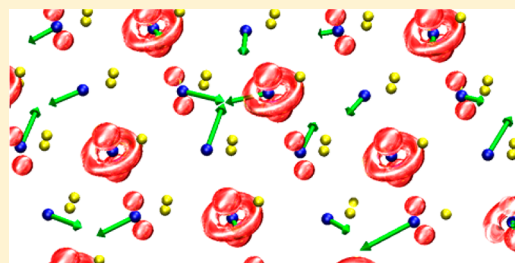
Bulk elemental and compound semiconductors have provided the basis for an astounding array of information technology devices over the last half century. However, improvements in miniaturization and efficiency have plateaued as we reach the limit at which three-dimensional structures cannot get any smaller without beginning to experience quantum confinement in one or more degrees of freedom. As a result, smaller, faster, low-power, flexible, or transparent devices may require a paradigm shift from three-dimensional to two-dimensional (2D) components.

Of particular interest for such 2D device components are atomically thin layers of transitional metal dichalcogenide (TMDC) semiconductors, which are chemically stable, have high carrier mobilities,[1,2] and can be synthesized using simple chemical vapor deposition (CVD) methods. These monolayers demonstrate 2D quantum confinement, possessing electronic structure and properties not observed in their bulk counterparts. Examples include emergent valley- and spin-dependent optical and electrical properties,[3−7] making these monolayers suitable for valleytronics; tunable semiconducting and metallic structural phases,[8−11] potentially useful for phase change memories; and strong light−matter interactions,[12,13] which hold promise for the use of 2D TMDCs in photonics and photocatalytic applications.[14,15] Finally, their resilience to large elastic strain[16−19] speaks to their potential in transparent and flexible electronic devices. Exploiting these unique properties

for the construction of novel electronic devices requires the functionalization of 2D and layered materials, as well as the construction of low-resistance ohmic contacts for their integration into electronic devices.

Optical control of structure and properties of TMDC monolayers is a potential route for functionalizing them, where the goal is to optically control electronic excitation in order to rapidly induce desired electronic and structural properties. Electronic excitation has previously been shown to induce bond dissociation and atomic rearrangement on ultrafast time scales in other material systems like graphene,[20] carbon nanotubes,[21] transition metal oxides,[22] and polymers.[23] Recent experiments on TMDC layers have shown strong response of atomic structures to optical and electronic excitation,[24,25] often characterized by the activation of specific lattice vibration modes. In particular, ultrafast electron diffraction experiments on MoSe₂ bilayers have shown picosecond conversion of electronic-excitation energy to thermal energy of the lattice with nearly perfect quantum yield.[26] Such ultrafast energy conversion is necessary for optical control of structural phase change in materials, with use in new applications such as phase
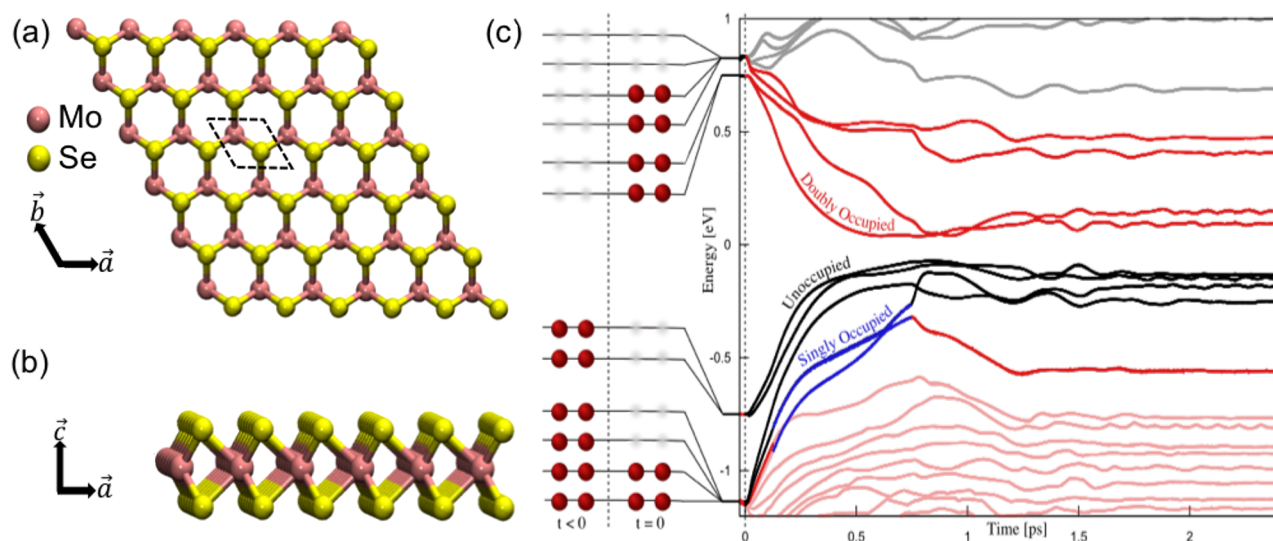
Figure 1. (a) Top and (b) side views of the simulated MoSe$_2$ monolayer. (c) Schematic of the simulated photoexcitation (left), and time evolution of the resulting electronic energies and occupations (right). Here, eight electrons from the valence-band maximum are promoted to the four levels at the conduction-band minimum. Red, blue, and black lines denote electronic levels occupied by two electrons, single electron, and no electron, respectively. Electronic levels with nontrivial dynamics are shown in thick lines.

change memories and neuromorphic computing.[27] This remarkable conversion ratio was attributed to strong electron−phonon coupling and the softening of acoustic phonons. This strong electron−phonon coupling in TMDCs has been observed not only in experiment but also in theoretical simulations.[28−33] However, the origin of the strong electron−phonon coupling upon photoexcitation, which is responsible for ultrafast nonradiative relaxation, has not been fully elucidated. A more complete understanding could allow for tailoring the electron−phonon coupling, thus enabling control of the atomic dynamics responsible for lattice thermalization and phase transformation.

Here, we study electronic and lattice dynamics of a model TMDC monolayer, MoSe$_2$, upon electronic excitation, using nonadiabatic quantum molecular dynamics (NAQMD) simulations[34] based on time-dependent density functional theory density, along with density functional theory (DFT) calculations. Our results show sub-picosecond transfer of electronic-excitation energy to lattice distortion manifested in the Debye−Waller factor (DWF). Sub-picosecond disordering is observed in both a free-standing monolayer, as well as a monolayer in contact with a heat bath, which is qualitatively similar to the more realistic situation of a monolayer on a substrate. The sub-picosecond disordering is preceded by softening of certain phonon modes at the Brillouin zone boundary.

Characterization of the monolayer's electronic structure in reciprocal space reveals that the strong electron−phonon coupling, indicated by the softened phonon modes, correlates well with the nesting vectors of the pocket-like, excited-state Fermi surface.

The simulated system is a monolayer of MoSe$_2$ with 108 atoms, comprising $6 \times 6 \times 1$ unit cells in the a-, b-, and c-directions, respectively. As shown in Figure 1a,b, each monolayer unit cell consists of one molybdenum atom sandwiched by two selenium atoms. Here, the c-axis is normal to the monolayer surface. NAQMD simulations[34] provide the dynamics of the coupled electron−ion system, where ionic dynamics are derived from the Hellman−Feynman theorem

(i.e., ionic trajectories are propagated using Newtonian mechanics based on quantum mechanically derived forces), electronic dynamics are modeled within the time-dependent DFT framework, and nonadiabatic transitions of electrons between energy bands are computed using the surface hopping approach. Optical excitation is modeled in our NAQMD simulations by instantaneously promoting a fixed number of electrons from the top of the valence band to the bottom of the conduction band, shown schematically in Figure 1c. This scheme for electronic excitation does not consider the complex interaction of light-fields with matter[35] as well as the process of hot-electron relaxation to the band edge, both of which occur on time-scales far shorter (few attoseconds to few femto-seconds) than those encountered in phonon dynamics, which are the focus of this Letter. Initially, eight electrons are promoted from the four bands at the valence-band maximum to the four at the conduction-band minimum, as shown at time $t = 0$ ps in Figure 1c. At time $t \approx 0.1$ ps, an electron from a doubly occupied band hops to an unoccupied band, resulting in these bands each becoming singly occupied. The excited electronic states are represented in terms of ground-state Kohn−Sham (KS) orbitals within DFT. The projector augmented wave method is used to compute the electronic states, where projector functions are generated for the 4d, 5s, and 5p states of Mo and 3d, 4s, and 4p states of Se. For the exchange-correlation energy, we employ the generalized gradient approximation, considering nonlinear core correc-tions. Electronic pseudowave functions and the pseudocharge density are represented by plane waves with respective cutoff energies of 30 and 250 Ry (408 and 3401 eV). A preconditioned conjugate gradient method is used to iteratively minimize the energy as a functional of KS orbitals.

We perform molecular dynamics (MD) simulations in both the canonical and microcanonical ensembles with a unit time step of 50 au (∼1.2 fs) and 8 au (∼0.2 fs), respectively. During simulation, periodic boundary conditions are applied in all directions. To prevent periodic images of the monolayer from interacting with one another, we add a vacuum layer of thickness 10 Å in the z-direction. We simulate nonadiabatic

electron−ion dynamics upon photoexcitation by alternating steps: (1) update transition probabilities between electronic excited states due to ionic motions using a surface-hopping procedure and (2) update ionic configuration due to new excited electronic states by numerically integrating MD equations.

In addition to ionic dynamics, the electronic structure and lattice stability in the excited state were characterized through the electronic band structure, wave function isosurfaces, charge densities, and phonon dispersion curves. Excited-state Fermi surfaces were plotted as reciprocal-space isosurfaces at energy levels corresponding to representative charge carrier concentrations of 0.2, 1, and 2×10^{14} cm^{-2} using the Wannier90 package.[36] Phonon dispersion curves were produced using DFT implemented in the Vienna Ab initio Simulation Package (VASP)[37−39] to corroborate the prediction that the emergence of Fermi surface nesting leads to phonon softening. Static calculations were performed on a $6 \times 6 \times 1$ supercell of a monolayer MoSe$_2$ crystal structure, containing 108 atoms, in both its electronic ground state, as well as at two different electronically excited states. The wave functions of valence electrons were constructed with a plane wave basis set with a kinetic energy cutoff of 520 eV. Reciprocal space was sampled using a $3 \times 3 \times 1$ Monkhorst−Pack k-point mesh with a Gaussian smearing of orbital occupancies of 0.1 eV. DFT perturbation theory within VASP was used to calculate the Hessian matrix, which was fed into the open-source phonopy[40] package to generate the dispersion relations for the normal vibration modes of the MoSe$_2$ unit cell. The electronically excited states were modeled using the ΔSCF method, where electrons are promoted from the highest-lying, occupied KS energy levels in the ground state, to the lowest-lying, unoccupied energy levels. We model the two different electronic excitations by moving one or two electrons from the valence band to the conduction band, equating to an electron−hole concentration of 0.297×10^{14} and 1.19×10^{14} cm^{-2}, respectively.

To predict the photoexcitation dynamics of suspended monolayers, in the absence of energy dissipation to or interaction with a substrate or heat bath, NAQMD is first carried out within the microcanonical ensemble. We excite electrons from the top two valence bands, which we denote as the valence band maximum (VBM), to the bottom two conduction bands, which we denote as the conduction band minimum (CBM). In total, four electrons are excited, corresponding to an excited charge carrier density of 1.19×10^{14} cm^{-2}. Figure 2 shows the electronic band structure and partial density of states (DOS) for the d-orbitals of Mo, which are the predominant orbitals making up the VBM and CBM, as well as charge densities for the VBM and CBM. The band structure plot is color coded to show the dominant d-orbital characters along the high symmetry lines in the first Brillouin zone.

We observe that the highest point in the VBM is the K-point (marked in Figure 2a with a green, dashed circle), with majority d$_{xy}$ and d$_{x^2-y^2}$ character. The lowest point in the CBM is also the K-point (marked in Figure 2a with a red, dashed circle), but is mainly of d$_{z^2}$ character. The iso-surfaces of the charge densities of the VBM and CBM, shown in Figure 2b, agree well with this orbital character assessment, with the CBM charge density showing the characteristic d$_{z^2}$ distribution, while the VBM charge density shows the signature d$_{xy}$ and d$_{x^2-y^2}$ shapes. During optical excitation, electrons that are excited
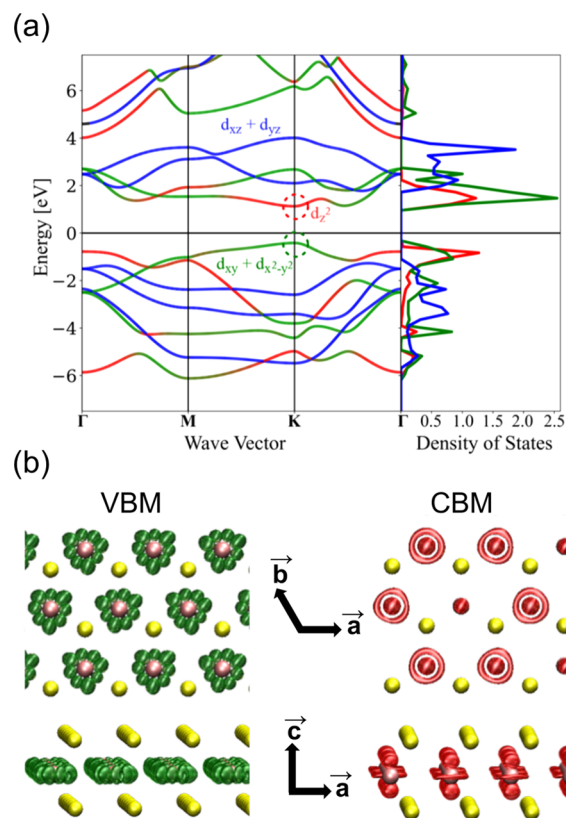
Figure 2. Electronic structure of monolayer MoSe$_2$. (a) Band structure plot denoting by color the character of the Mo d-orbitals that make up the majority of the state at each point, as well as a partial density of states of the different d-orbitals of Mo. The top valence (conduction) band is denoted with a green (red), dashed circle, indicating the state is predominantly composed of d$_{z^2}$ (d$_{xy}$ and d$_{x^2-y^2}$) orbitals. (b) Charge densities for the top two valence bands and the bottom two conduction bands, showing how the electronic charge density changes when we excite electrons from their ground state.

from the VBM to the CBM remain spatially localized around Mo atoms. However, while they are formerly localized in d$_{xy}$ and d$_{x^2-y^2}$ orbitals in the $x−y$ plane, excitation promotes them into d$_{z^2}$ orbitals that spread along the z-direction. Since both VBM and CBM are at the K-point in reciprocal space, the monolayer exhibits a direct band gap, in agreement with experiments.[41]

To quantify lattice disorder along a given reciprocal vector $\vec{q}$, we compute the Debye−Waller Factor (DWF) as a function of time t:

$$\mathrm{DWF} = e^{-\langle |\vec{q} \cdot \vec{u}(t)|^2 \rangle}$$

where $\vec{u}(t)$ is the displacement vector of an atom from its original position at $t = 0$, and the brackets $\langle \rangle$ denote an average over all atoms in the supercell.

Figure 3 shows time evolution of the DWF for the monolayer with electronic excitation (red line) along two representative directions in hexagonal 2D crystals, the zigzag direction (300) and the armchair direction (110), compared to an unexcited monolayer at 10 K (blue line). The relative lack of atomic motion at 10 K results in a near-unity value for the DWF. DWF values for the room temperature crystal can be found in Figure S1 in the Supporting Information. Our results predict a sub-picosecond, exponential decay of the DWF along both the (110) and (300) planes upon electron excitation.
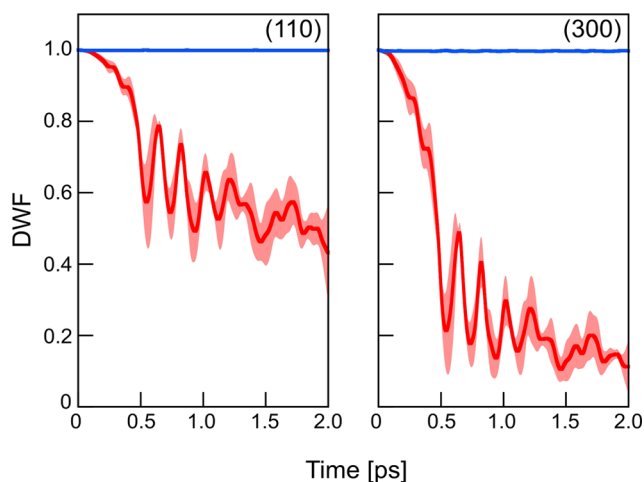
Figure 3. Time evolution of Debye−Waller factor along the (110) and (300) planes, with (red) and without (blue) photoexcitation, averaged over three simulation runs beginning from identical positions but different initial velocities in the microcanonical ensemble. The shading shows the standard deviation across the three independent simulations.

Further, we also observe a high-frequency modulation in the DWF for times t = 0.5 to 1.5 ps after excitation. These high-frequency features (Figure 4c) with a time period of 0.2 ps correspond to the emission of coherent phonons with ω = 2.5 THz, which falls within the range of softened vibrational frequencies for acoustic modes at the M- and K-points in reciprocal space. These vibration modes possess strong electron−phonon coupling and large phonon line widths and are therefore preferentially excited in electron-doped or optically excited TMDC crystals.[42] Further, these high-frequency vibrations are quenched after ~1 ps, which is consistent with recent experimental work on photoexcited atomically thin $MoSe_2$, which demonstrated ultrafast lattice thermalization.[26] These experiments suggest that the under-lying cause for such rapid onset of electronic excitation induced lattice disorder is strong electron−phonon coupling.[26] To aid in confirming this conclusion, we investigate the electronic structure, and specifically the Fermi surface, of the photoexcited $MoSe_2$ monolayer.

Figure 4a shows the total DOS (blue line) for electrons in the monolayer TMDC system, as well as the integrated DOS (red line), which is used to compute the Fermi surface at different electron−hole concentrations. Contours of these Fermi surfaces at varying levels of electronic excitation are
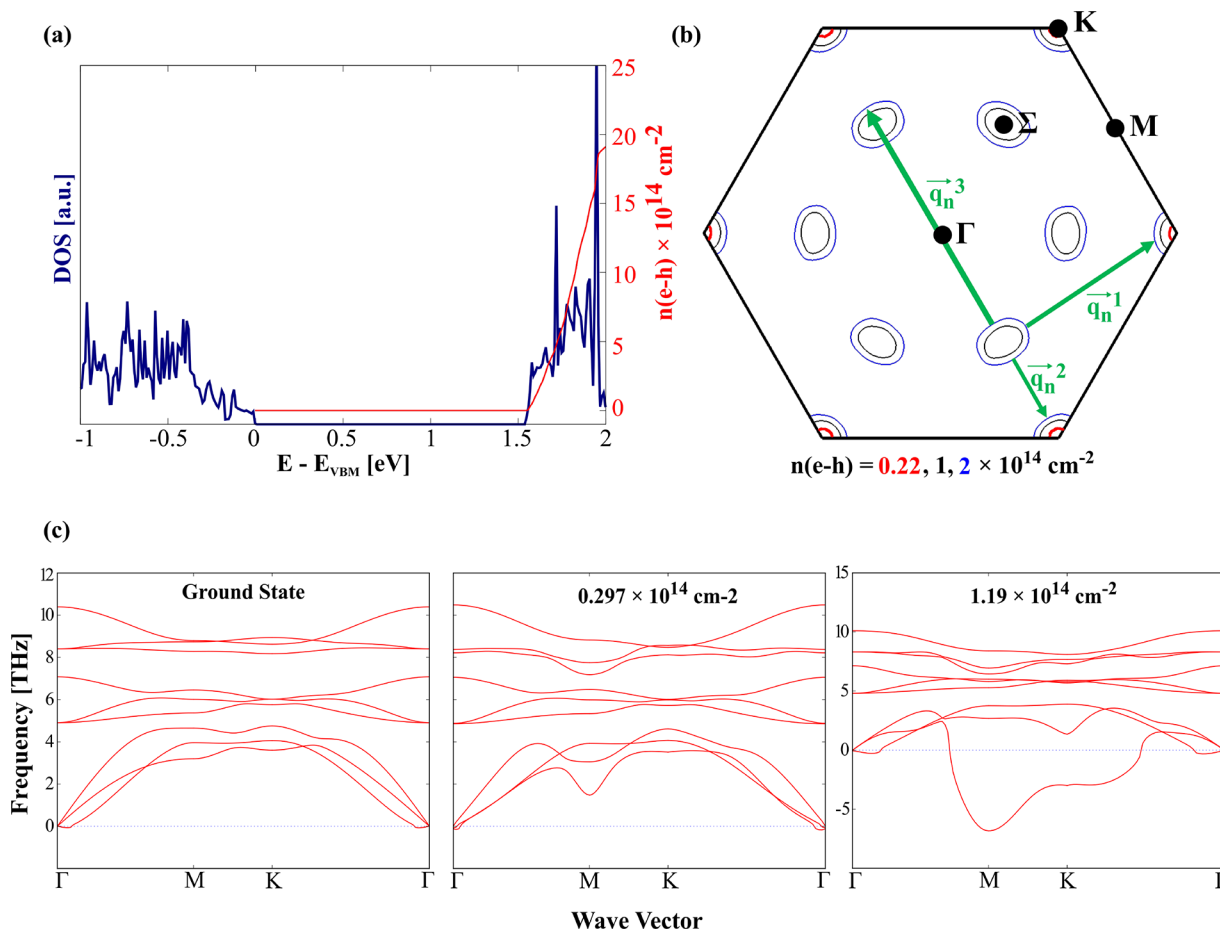

Figure 4. (a) Electronic density of states of $MoSe_2$ monolayer near the band edge (blue line). Red line shows integrated density of states, which is used to determine the Fermi level for a given value of electron−hole pair density, $n(e−h)$. (b) Fermi surface for excited carrier density, $n(e−h)$, values ranging from 0 to 2×10^{14} cm^{-2}. The Fermi surface is localized at the K-points at minimal excitation (red contours), while exposing Σ-pockets at higher excited electron−hole densities (black and blue contours). The three nesting vectors $\vec{q}_n^1$, $\vec{q}_n^2$, and $\vec{q}_n^3$ correspond to reciprocal vectors ΓM, ΓK, and $\Gamma \Sigma$, respectively. (c) Phonon dispersion curves in the ground state and two increasingly excited states.

shown in Figure 4b. We see that at minimal excitation, the Fermi surface is localized around the K (1/3, 1/3, 0) point in the Brillouin zone. However, upon stronger photoexcitation the Fermi surface develops pockets between the Γ (0, 0, 0) and K (1/3, 1/3, 0) points, usually denoted as the Σ point. Similar behavior is observed for other monolayer materials in the TMDC family upon electronic excitation or charge doping.[42,43] With these pockets come parallel (nested) sheets of Fermi surface and the Fermi surface nesting vectors that connect them. Such nesting greatly increases the number of possible electronic transitions at the nesting wave vectors and causes phonon softening at corresponding points on momentum space. Indeed, calculated phonon dispersion curves for the monolayer of $MoSe_2$ show phonon softening upon photo-excitation. Figure 4c shows the phonon dispersion curves for the ground state and two different excited states along lines of high symmetry in reciprocal space. The phonon dispersion curve for the ground state exhibits all positive frequencies, indicating the stability of the structure in this state. However, with mild excitation, we begin to observe zone-edge phonon softening at the M point in the Brillouin zone. Upon higher excitation, we see additional phonon softening at the K point as well as a uniform decrease in atomic vibration frequencies throughout the Brillouin zone, which reflects a weakening of interatomic bonds and leads to larger atomic displacements (i.e., decreasing DWF values as observed in the NAQMD simulations).

It is important to note that dynamics resulting from softening of both the M-point and K-point vibration modes can be observed only in supercells commensurate with the periodicity of both vibration modes. The $6 \times 6 \times 1$ supercell considered in this study is the smallest system that is compatible with both these modes. Smaller simulation cells like $4 \times 4 \times 1$ show qualitatively different atomic displacements upon electronic excitation (see Supporting Videos 1 and 2) due to their inability to accommodate all softened vibration modes, which results in different time constants for decay of the Debye–Waller factor (Figure S1 in the Supporting Information).

The onset of softened phonon modes can be attributed to strong electron–phonon coupling in the material,[44,45] which in turn provides a pathway for extremely efficient, nonradiative relaxation of excited carrier energy into lattice disorder. This provides an explanation for the ultrafast conversion of electronic energy into atomic motion as observed by the sub-picosecond decay in the DWF.

While these microcanonical NAQMD simulations most closely model suspended monolayers, supported monolayers that would be found in functionalized devices are more closely simulated with canonical NAQMD. This is because the substrate on which a monolayer is placed can affect the molecular dynamics through modified electron–hole screening as well as acting as a weak heat bath for the excited monolayer. Canonical ensemble NAQMD simulations, where the excited monolayer is coupled to a Nosé–Hoover heat bath, can model the latter effect. Figure 5 shows the DWF versus time, in the (110) and (300) directions at two different electron–hole concentrations. We observe that the large decay in DWF, reflecting significant lattice disorder, persists despite the coupling to a thermostat at 10 K indicating that atomic motion in the deformed electronic potential energy surface dominates lattice order on ps time scales after photoexcitation. Furthermore, we see an increase in the amount of lattice
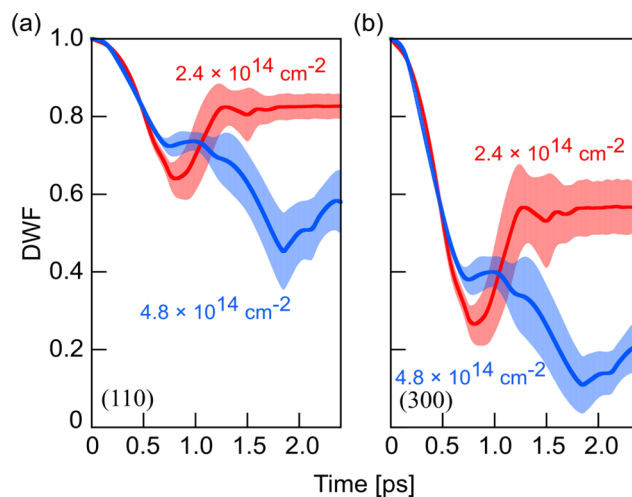

Figure 5. Debye–Waller factor plotted versus time along the (110) (a) and (300) (b) planes, at two different electron–hole densities, in the canonical ensemble.

disorder with increased electron–hole density. This finding is validated by recent experimental work, which found similar dynamics.[26]

In conclusion, NAQMD simulations were performed to model photoexcitation of monolayer $MoSe_2$ crystals in the microcanonical and canonical ensembles. Electronic structure characterization reveals that electronic excitation leads to the formation of pocket-like Fermi surface states, which are connected by nesting vectors that correspond closely to wave vectors of softened phonon modes, indicating strong electron–phonon coupling. Sub-picosecond decay of the Debye–Waller factor was observed in both ensembles, indicating ultrafast transfer of optical energy to thermal motion. Such rapid disordering of the $MoSe_2$ lattice has important implications for optically controlling structure and properties of TMDC monolayers.

■ ASSOCIATED CONTENT

ⓢ Supporting Information

The Supporting Information is available free of charge on the ACS Publications website at DOI: 10.1021/acs.nanolett.8b00474.

> Explanation for the simulation cell size effect, including a plot showing how the structural dynamics vary for different sized simulation cells upon the same level of photoexcitation (PDF)
>
> Video showing the lattice dynamics of the 48-atom system (MPG) and 108-atom system (MPG) upon photoexcitation, including visualization of antibonding and displacement vectors

■ AUTHOR INFORMATION

Corresponding Author

*E-mail: priyav@usc.edu. Fax: +1 (213) 821-2664.

ORCID Ⓘ

Lindsay Bassman: 0000-0003-3542-1553

Aravind Krishnamoorthy: 0000-0001-6778-2471

Aiichiro Nakano: 0000-0003-3228-3896

Priya Vashishta: 0000-0003-4683-429X

■ ABBREVIATIONS

TMDC, transition metal dichalcogenide; 2D, two-dimensional; DFT, density functional theory; NAQMD, nonadiabatic quantum molecular dynamics; KS, Kohn−Sham; MD, molecular dynamics; DWF, Debye−Waller factor; UED, ultrafast electron diffraction

■ REFERENCES

(1) Podzorov, V.; Gershenson, M.; Kloc, C.; Zeis, R.; Bucher, E. *Appl. Phys. Lett.* **2004**, *84*, 3301−3303.

(2) Schmidt, H.; Wang, S.; Chu, L.; Toh, M.; Kumar, R.; Zhao, W.; Castro Neto, A.; Martin, J.; Adam, S.; Özyilmaz, B. *Nano Lett.* **2014**, *14*, 1909−1913.

(3) Cao, T.; Wang, G.; Han, W.; Ye, H.; Zhu, C.; Shi, J.; Niu, Q.; Tan, P.; Wang, E.; Liu, B. *Nat. Commun.* **2012**, *3*, 887.

(4) Mak, K. F.; He, K.; Shan, J.; Heinz, T. F. *Nat. Nanotechnol.* **2012**, *7*, 494−498.

(5) Zeng, H.; Dai, J.; Yao, W.; Xiao, D.; Cui, X. *Nat. Nanotechnol.* **2012**, *7*, 490−493.

(6) Mannebach, E. M.; Duerloo, K.-A. N.; Pellouchoud, L. A.; Sher, M.-J.; Nah, S.; Kuo, Y.-H.; Yu, Y.; Marshall, A. F.; Cao, L.; Reed, E. J. *ACS Nano* **2014**, *8*, 10734−10742.

(7) Xiao, D.; Liu, G.-B.; Feng, W.; Xu, X.; Yao, W. *Phys. Rev. Lett.* **2012**, *108*, 196802.

(8) Voiry, D.; Yamaguchi, H.; Li, J.; Silva, R.; Alves, D. C.; Fujita, T.; Chen, M.; Asefa, T.; Shenoy, V. B.; Eda, G. *Nat. Mater.* **2013**, *12*, 850−855.

(9) Eda, G.; Fujita, T.; Yamaguchi, H.; Voiry, D.; Chen, M.; Chhowalla, M. *ACS Nano* **2012**, *6*, 7311−7317.

(10) Lin, Y.-C.; Dumcenco, D. O.; Huang, Y.-S.; Suenaga, K. *Nat. Nanotechnol.* **2014**, *9*, 391−396.

(11) Duerloo, K.-A. N.; Li, Y.; Reed, E. J. *Nat. Commun.* **2014**, *5*, 4214.

(12) Britnell, L.; Ribeiro, R.; Eckmann, A.; Jalil, R.; Belle, B.; Mishchenko, A.; Kim, Y.-J.; Gorbachev, R.; Georgiou, T.; Morozov, S. *Science* **2013**, *340*, 1311−1314.

(13) Bernardi, M.; Palummo, M.; Grossman, J. C. *Nano Lett.* **2013**, *13*, 3664−3670.

(14) Mak, K. F.; Shan, J. *Nat. Photonics* **2016**, *10*, 216−226.

(15) Cao, L. *MRS Bull.* **2015**, *40*, 592−599.

(16) Bertolazzi, S.; Brivio, J.; Kis, A. *ACS Nano* **2011**, *5*, 9703−9709.

(17) Feng, J.; Qian, X.; Huang, C.-W.; Li, J. *Nat. Photonics* **2012**, *6*, 866−872.

(18) Yu, D.; Feng, J.; Hone, J. *MRS Bull.* **2014**, *39*, 157−162.

(19) Van Der Zande, A.; Hone, J. *Nat. Photonics* **2012**, *6*, 804−806.

(20) Bang, J.; Meng, S.; Sun, Y.-Y.; West, D.; Wang, Z.; Gao, F.; Zhang, S. *Proc. Natl. Acad. Sci. U. S. A.* **2013**, *110*, 908−911.

(21) Zhang, J.; Wang, R.; Zhu, X.; Pan, A.; Han, C.; Li, X.; Zhao, D.; Ma, C.; Wang, W.; Su, H. *Nat. Commun.* **2017**, *8*, 683.

(22) Kolesov, G.; Vinichenko, D.; Tritsaris, G. A.; Friend, C. M.; Kaxiras, E. *J. Phys. Chem. Lett.* **2015**, *6*, 1624−1627.

(23) Bealing, C. R.; Ramprasad, R. *J. Chem. Phys.* **2013**, *139*, 174904.

(24) Mannebach, E. M.; Li, R.; Duerloo, K.-A.; Nyby, C.; Zalden, P.; Vecchione, T.; Ernst, F.; Reid, A. H.; Chase, T.; Shen, X. *Nano Lett.* **2015**, *15*, 6889−6895.

(25) Cho, S.; Kim, S.; Kim, J. H.; Zhao, J.; Seok, J.; Keum, D. H.; Baik, J.; Choe, D.-H.; Chang, K.; Suenaga, K. *Science* **2015**, *349*, 625−628.

(26) Lin, M.-F.; Kochat, V.; Krishnamoorthy, A.; Bassman, L.; Weninger, C.; Zheng, Q.; Zhang, X.; Apte, A.; Tiwary, C. S.; Shen, X.; Li, R.; Kalia, R. K.; Ajayan, P.; Nakano, A.; Vashishta, P.; Shimojo, F.; Wang, X.; Fritz, D. M.; Bergmann, U. *Nat. Commun.* **2017**, *8*, 1745.

(27) Sangwan, V. K.; Lee, H.-S.; Bergeron, H.; Balla, I.; Beck, M. E.; Chen, K.-S.; Hersam, M. C. *Nature* **2018**, *554*, 500.

(28) Szabó, Á.; Rhyner, R.; Luisier, M. *Phys. Rev. B: Condens. Matter Mater. Phys.* **2015**, *92*, 035435.

(29) Gunst, T.; Markussen, T.; Stokbro, K.; Brandbyge, M. *Phys. Rev. B: Condens. Matter Mater. Phys.* **2016**, *93*, 035414.

(30) Li, W. *Phys. Rev. B: Condens. Matter Mater. Phys.* **2015**, *92*, 075405.

(31) Li, L.; Long, R.; Prezhdo, O. V. *Chem. Mater.* **2017**, *29*, 2466−2473.

(32) Li, L.; Long, R.; Bertolini, T.; Prezhdo, O. V. *Nano Lett.* **2017**, *17*, 7962−7967.

(33) Wei, Y.; Li, L.; Fang, W.; Long, R.; Prezhdo, O. V. *Nano Lett.* **2017**, *17*, 4038−4046.

(34) Shimojo, F.; Hattori, S.; Kalia, R. K.; Kunaseth, M.; Mou, W.; Nakano, A.; Nomura, K.-i.; Ohmura, S.; Rajak, P.; Shimamura, K. *J. Chem. Phys.* **2014**, *140*, 18A529.

(35) Bostrom, E. V.; Mikkelsen, A.; Verdozzi, C.; Perfetto, E.; Stefanucci, G. *Nano Lett.* **2018**, *18*, 785−792.

(36) Mostofi, A. A.; Yates, J. R.; Pizzi, G.; Lee, Y.-S.; Souza, I.; Vanderbilt, D.; Marzari, N. *Comput. Phys. Commun.* **2014**, *185*, 2309−2310.

(37) Kresse, G.; Hafner, J. *Phys. Rev. B: Condens. Matter Mater. Phys.* **1993**, *47* (1), 558.

(38) Kresse, G.; Furthmüller, J. *Comput. Mater. Sci.* **1996**, *6*, 15−50.

(39) Kresse, G.; Furthmüller, J. *Phys. Rev. B: Condens. Matter Mater. Phys.* **1996**, *54*, 11169.

(40) Togo, A.; Tanaka, I. *Scr. Mater.* **2015**, *108*, 1−5.

(41) Zhang, Y.; Chang, T.-R.; Zhou, B.; Cui, Y.-T.; Yan, H.; Liu, Z.; Schmitt, F.; Lee, J.; Moore, R.; Chen, Y. *Nat. Nanotechnol.* **2014**, *9*, 111−115.

(42) Zeng, S.; Zhao, Y.; Li, G.; Ni, J. *Phys. Rev. B: Condens. Matter Mater. Phys.* **2016**, *94*, 024501.

(43) Krishnamoorthy, A.; Bassman, L.; Kalia, R.; Nakano, A.; Shimojo, F.; Vashishta, P. *Nanoscale* **2018**, *10*, 2742−2747.

(44) Allen, P. B.; Cohen, M. L. *Phys. Rev. Lett.* **1972**, *29*, 1593.

(45) Moussa, J. E.; Cohen, M. L. *Phys. Rev. B: Condens. Matter Mater. Phys.* **2006**, *74*, 094520.